Phase diagram of the spin-$\frac{1}{2}$ Yukawa–Sachdev-Ye-Kitaev model: Non-Fermi liquid, insulator, and superconductor

Wei Wang [1,2,*] Andrew Davis [3,*] Gaopei Pan [1,2] Yuxuan Wang [3,†] and Zi Yang Meng [4,1,‡]

[1]*Beijing National Laboratory for Condensed Matter Physics and Institute of Physics, Chinese Academy of Sciences, Beijing 100190, China*

[2]*School of Physical Sciences, University of Chinese Academy of Sciences, Beijing 100190, China*

[3]*Department of Physics, University of Florida, Gainesville, Florida 32601, USA*

[4]*Department of Physics and HKU-UCAS Joint Institute of Theoretical and Computational Physics, The University of Hong Kong, Pokfulam Road, Hong Kong SAR, China*

(Received 18 February 2021; revised 17 April 2021; accepted 19 April 2021; published 5 May 2021)

We analyze the phase diagram of the spin-$\frac{1}{2}$ Yukawa–Sachdev-Ye-Kitaev model, which describes complex spin-$\frac{1}{2}$ fermions randomly interacting with real bosons via a Yukawa coupling, at finite temperatures and varying fermion density. A recent work [Wang and Chubukov, Phys. Rev. Res. **2**, 033084 (2020).] showed that, upon varying the filling or chemical potential, a first-order quantum phase transition exists between a non-Fermi-liquid (NFL) phase and an insulating phase. Here we show that in such a model with time-reversal symmetry this quantum phase transition is preempted by a pairing phase that develops as a low-temperature instability. As a remnant of the would-be NFL-insulator transition, the superconducting critical temperature rapidly decreases beyond a certain chemical potential. On the other hand, depending on the parameters, the first-order quantum phase transition extends to finite temperatures and terminates at a thermal critical point, beyond which the NFL and the insulator become the same phase, similar to that of the liquid-gas and metal-insulator transition in real materials. We determine the pairing phase boundary and the location of the thermal critical point via combined analytic and quantum Monte Carlo numeric efforts. Our results provide a model realization of the transition of NFLs towards superconductivity and insulating states and therefore offer a controlled platform for future investigations of the generic phase diagram that hosts a NFL, insulator, and superconductor and their phase transitions.

DOI: 10.1103/PhysRevB.103.195108

I. INTRODUCTION

Understanding the non-Fermi-liquid (NFL) behavior of interacting electron systems is one of the central issues in modern condensed-matter physics. Widely believed to be relevant to the microscopic origin of the strange metal behavior in unconventional superconductors [1–8], its theoretical description remains a challenging issue due to the lack of a small control parameter. Recently, the Sachdev-Ye-Kitaev (SYK) model has garnered widespread attention as it has emerged as a new paradigm for the study of NFLs [9–12], which is different from most previous research of NFLs, where the system is usually realized in itinerant fermions coupled to soft bosonic modes near a quantum critical point [13–20]. The NFL in SYK model is exactly solvable in the large-N limit. Beyond the context of non-Fermi liquids, the SYK model has also been found to have a hidden holographic connection to quantum black holes and saturates the limiting rate of scrambling due to its short equilibration time [21,22].

Motivated by the aforementioned fermionic systems near quantum critical points, recently, a variant of the SYK model, dubbed the Yukawa-SYK model, was proposed [23–27]. Such a model describes strong random Yukawa coupling between MN flavors of fermions and N^2 flavors of bosons. Analytical investigation at large N has revealed a saddle point solution in which the Yukawa coupling "self-tunes" the massive bosons to criticality and the fermions form a NFL, which saturates the bound on quantum chaos [28,29]. This saddle point solution has been verified at finite N and finite T via quantum Monte Carlo (QMC) simulations with an additional antiunitary time-reversal symmetry [27] by making use of a reparametrization symmetry of the large-N solution.

In this work we focus on the fate of the NFL upon varying temperature and density. Similar to the discovery of the complex SYK model [30,31], it was recently shown that a first-order quantum phase transition exists at finite chemical potential separating a NFL state and a gapped insulating state [23]. On the other hand, in several versions of the Yukawa-SYK model and the complex SYK model, the NFL phase becomes unstable to a pairing phase [24–26,32–34]. In particular for the Yukawa-SYK models [23–27], two distinct pairing behaviors have been reported, depending on whether fermions carry spin degrees of freedom. For the spinless Yukawa-SYK model studied in Ref. [24], it was found that pairing occurs only for a certain range of the ratio between boson and fermion flavor numbers, while for spin-$\frac{1}{2}$ Yukawa-SYK models [25–27], the NFL state

*These authors contributed equally to this work.

†yuxuan.wang@ufl.edu

‡zymeng@hku.hk

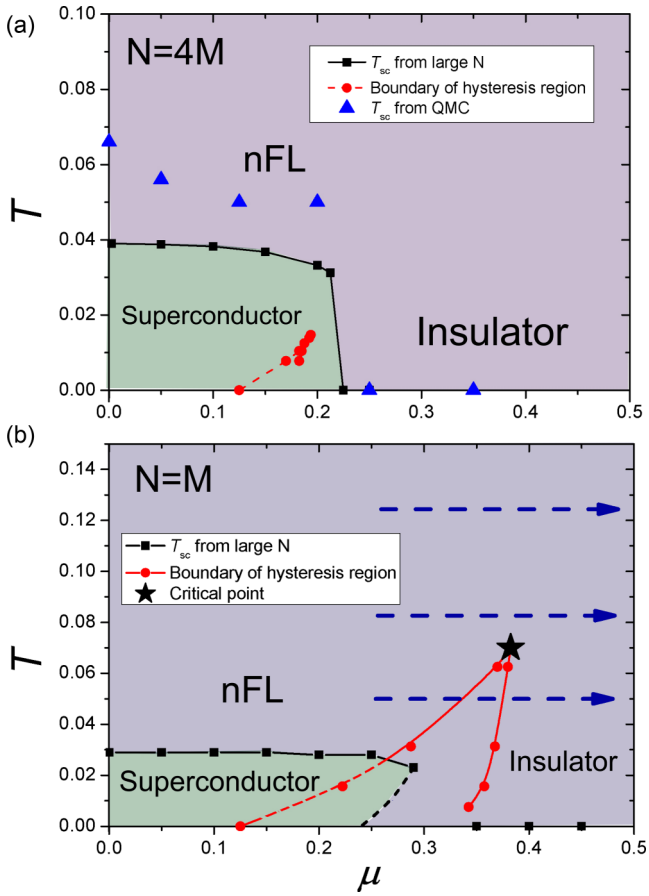

FIG. 1. (a) Phase diagram of the Yukawa-SYK model at $N = 4M$, $\omega_0 = 1$, $m_0 = 2$. From the large-N calculation, one sees the NFL become a superconductor at low temperature in a wide range of the chemical potential and the first-order hysteresis region denoted by the red points and lines, obtained in the absence of pairing instability within large N. In the presence of superconductivity the position of this region is renormalized, hence the dashed line. The thermal critical point that terminates the first-order transition locates at ($\mu_c = 0.194$, $T_c = 0.015$). The blue triangles are the transition points from a NFL to a superconductor obtained from QMC at finite N, M (see Fig. 4), which are consistent with the results obtained from large-N calculations (black squares). (b) Phase diagram of the Yukawa-SYK model at $N = M$, $\omega_0 = 1$, $m_0 = 2$ from the large-N calculation. The first-order hysteresis region denoted by the red points and lines is obtained in the absence of pairing instability within large N. The dashed-line portion of this boundary is renormalized by superconductivity phase. The black dashed line denotes the boundary of the superconducting phase within the hysteresis region and is depicted only qualitatively. The QMC n-μ curves in Fig. 2 are along blue dashed paths. The thermal critical point at ($\mu_c = 0.3825$, $T_c = 0.07$) is denoted by the black star.

is, in general, unstable toward pairing at sufficiently low temperatures.

Here by means of large-N calculation and unbiased large-scale QMC simulation, we present the global phase diagram (see Fig. 1) of the spin-$\frac{1}{2}$ version of the Yukawa-SYK model, spanned by the axes of temperature T and chemical potential μ. Up to a critical value in the chemical potential μ, a finite-temperature phase transition from NFL to superconductivity is observed. We determine the pairing transition by solving the linear Eliashberg equation using the large-N result of the Green's functions, as well as finite-size scaling of the pairing susceptibility in QMC simulations. We obtain good agreement between the two methods, indicating the pairing transition is mean-field-like. In particular, in the weak-coupling limit, we analytically determine the threshold value for μ for the superconductor-insulator transition at zero temperature, which agrees well with numerical results. On the other hand, by solving the Schwinger-Dyson equation, we found the first-order quantum phase transition extends to low temperature and terminates at a (thermal) critical point, which is a generic feature in many metal-insulator transitions in correlated materials [35,36]. However, depending on the strength of the first-order quantum transition (previously found to be controlled by the ratio M/N [23]), we show that the thermal critical point may be masked by the superconducting phase. The phase diagram obtained offers a controlled platform for future investigations of phase transitions between a NFL, insulator, and superconductor at generic electron fillings.

II. THE SPIN-$\frac{1}{2}$ YUKAWA-SYK MODEL

The Yukawa-SYK model we study is described by the following Hamiltonian:

$$H = \sum_{i,j=1}^{M} \sum_{\alpha,\beta=1}^{N} \sum_{m,n=\uparrow,\downarrow} \left(\frac{i}{\sqrt{MN}} t_{i\alpha,j\beta} \phi_{\alpha\beta} c^{\dagger}_{i\alpha m} \sigma^{z}_{m,n} c_{j\beta n}\right) + \sum_{\alpha,\beta=1}^{N} \left(\frac{1}{2}\pi^{2}_{\alpha\beta} + \frac{m_0^2}{2}\phi^{2}_{\alpha\beta}\right) - \mu \sum_{i=1}^{M} \sum_{\alpha=1}^{N} \sum_{m=\uparrow,\downarrow} c^{\dagger}_{i\alpha m} c_{i\alpha m}, \tag{1}$$

where $c_{i\alpha m}$ ($c^{\dagger}_{i\alpha m}$) is the annihilation (creation) operator for a fermion with flavor α and spin m, n ($\uparrow$ or $\downarrow$). The random Yukawa coupling parameter between a fermion and a boson is realized as $\langle t_{i\alpha,j\beta}\rangle = 0$, $\langle t_{i\alpha,j\beta} t_{k\gamma,l\delta}\rangle = (\delta_{\alpha\gamma}\delta_{ik}\delta_{\beta\delta}\delta_{jl} + \delta_{\alpha\delta}\delta_{il}\delta_{\beta\gamma}\delta_{jk})\omega_0^3$. We set $\omega_0 = 1$ as the energy unit throughout the paper. The dynamical behavior of the boson is given in the second term, and $\pi_{\alpha\beta}$ is the canonical momentum of $\phi_{\alpha\beta}$. Hermiticity of the model requires $\phi_{\alpha\beta} = -\phi_{\beta\alpha}$. (α, β) are flavor indices which run from 1 to N, and (i, j) are quantum dot indices which run from 1 to M. σ^z represents the z component of the fermion spin. Due to time-reversal symmetry, this Hamiltonian is free from the fermion sign problem and can be simulated by QMC at finite M and N and at finite doping with $\mu \neq 0$. We prove the absence of the sign problem and discuss the QMC implementation in Appendix A.

As we mentioned, compared to the spinless Yukawa-SYK model previously studied [24], the key difference is the inclusion of the spin degree of freedom, which enables a sign-problem-free quantum Monte Carlo simulation of the model. Physically, this modification introduces an instability toward spin-singlet pairing, while in Ref. [24] the pairing of spinless fermions occurs at only certain regimes of (M, N). The behavior of the model (1) at $\mu = 0$ was studied in our previous work in Ref. [23], and in this work we focus on the phases for a generic μ.

The main results of this work can be summarized by the two representative phase diagrams. We found that, in general, a superconducting dome $T_{sc}(\mu)$ exists in the T-μ plane shown in Fig. 1 (the phases for positive and negative μ are identical by particle-hole symmetry). The vanishing of pairing for larger μ is driven by the underlying NFL/insulator transition. In the absence of pairing, we obtain a hysteresis region (the wedge region marked by red lines in Fig. 1) in which both the NFL and insulator states are metastable, divided by a first-order phase transition inside the wedge, similar to that of the liquid-gas transition and metal-insulator transition in many correlated materials [35,36]. The exact location of the first-order transition requires comparing the free energies of different solutions, which is beyond the scope of the current work. For $N = 4M$, $\omega_0 = 1$, $m_0 = 2$, the superconducting dome completely preempts the would-be NFL/insulator transition, while for $N = M$, $\omega_0 = 1$, $m_0 = 2$, the first-order phase transition is stronger and the corresponding thermal critical point occurs outside of the superconducting phase. In Fig. 1(a) we have also marked the superconducting critical temperature obtained by finite-size scaling from QMC data with blue triangles, which are consistent with the results obtained from large-N calculations denoted by the black squares. The exact position of the hysteresis region inside the superconducting phase and vice versa requires solving the nonlinear superconducting gap equation and is qualitatively marked by dashed lines.

III. PHASES IN THE NORMAL STATE

Within large N, we map out the T-μ phase diagram by numerically solving the Schwinger-Dyson equations (2). In terms of the propagators $G_f^{-1}(i\omega) = i\omega + \mu + \Sigma(i\omega)$ for the fermions and $G_b^{-1}(i\Omega) = \Omega^2 + m_0^2 + \Pi(i\Omega)$ for the bosons, the Schwinger-Dyson equations are

$$\Sigma(i\omega) = -\omega_0^3 \int \frac{d\Omega}{2\pi} G_b(i\Omega) G_f(i\omega - i\Omega),$$
$$\Pi(i\Omega) = \frac{4M}{N}\omega_0^3 \int \frac{d\omega}{2\pi} G_f(i\Omega/2 + i\omega) G_f(-i\Omega/2 + i\omega). \tag{2}$$

Since we work in the large-(M, N) regime, only the ratio M/N enters the equations [27].

We solve Eqs. (2) iteratively by starting with a simple ansatz for Σ_0 and Π_0 on the right-hand sides, obtaining updated values Σ_1 and Π_1 on the right-hand sides, and repeating until the solutions $\{\Sigma_n\}$ and $\{\Pi_n\}$ saturate, where n is the iteration step number. Noting that Eqs. (2) are consistent with the assumptions that $\Pi(i\Omega)$ is even and that the real and imaginary parts of $\Sigma(i\omega)$ are even and odd, respectively, we need to compute only the self-energies at nonnegative frequencies. However, directly implementing this strategy leads to divergent behavior, especially at $\Sigma_n(\pm\pi T)$ and $\Pi_n(0)$. This issue is related to the fact that $\Sigma_n(\pm\pi T)$ and $\Pi_n(0)$ are determined by the behaviors of G and D at all frequency scales, rather than their "local" behavior at nearby low energies [23]. Indeed, in analytical solutions of Eq. (1) at $T = 0$ [23], the conditions on $\Sigma(0)$ and $\Pi(0)$ were used to determine the ultraviolet energy scale beyond which NFL behavior crosses over to that of a free system. To avoid the instability at lowest frequency points in the iterative method, we artificially introduce the "stabilizers" for each step of the iteration by uniformly shifting Σ_n and Π_n such that

$$\Sigma_n'(\pi T) = s, \quad \Pi_n'(0) = p. \tag{3}$$

This prescription prevents $\Sigma_n(\pi T)$ and $\Pi_n(0)$ from running away. Of course, in general, after the iteration converges, the solution we get is *not* the solution of the original SD equation, unless the updated value at the next step coincides with the stabilizers, i.e., $\Sigma_{n+1}(\pi T) \to s$ and $\Pi_{n+1}(0) \to p$. Using this criterion, we can find the correct values of the stabilizers s_0 and p_0. The necessary shifts are typically extremely small compared to the values of the self-energies over the frequency range where most of their support lies.

At low T and for some ranges of μ, we obtain two different choices of stabilizers $\{s_0, p_0\}$ which cause the iteration to converge. This signals the hysteresis behavior, and the resulting two types of solutions physically correspond to NFL and insulator behaviors that are the local minimum of the free energy. This method does not reproduce the unstable $(dn/d\mu < 0)$ solutions, whose boundaries are sketched qualitatively in Fig. 2. The filling n is calculated from the imaginary-time fermionic

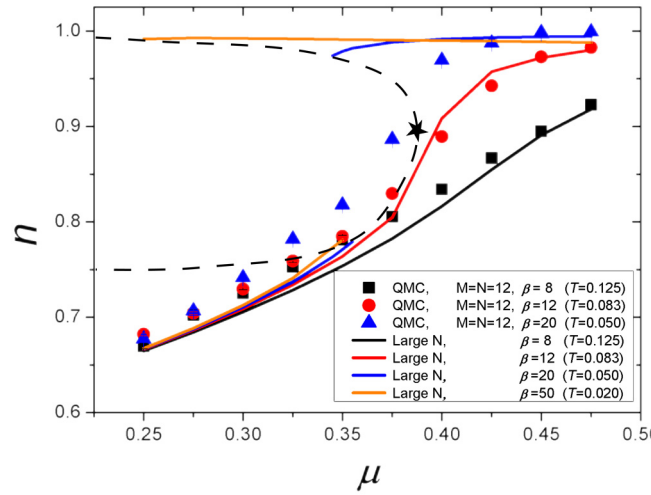

FIG. 2. Filling n versus μ for selected T in the vicinity of the thermal critical point in Fig. 1 (b) for $N = M$, $\omega_0 = 1$, $m_0 = 2$. At higher $T = 0.125$, one sees the $n(\mu)$ curves from both large N and QMC are smooth. $T = 0.125$, $\mu = 0.375$ (marked by the star) is a thermal critical point. At temperature $T = 0.083$ close to the thermal critical point, there is a sharp turn in $n(\mu)$ signifying the divergence of the compressibility $dn/d\mu$. At lower T, there is a range of μ—the hysteresis region—where the filling is double valued. The lower branch represents the NFL behavior, and the upper branch represents the insulating behavior; a first-order transition connects the two at a chemical potential given by a Maxwell construction. The dashed line delimits the region where solutions are unstable. Note that the QMC results at $T = 0.050$ (the blue triangles) further differ from the first-order transition behavior (the blue curves). At finite M, N and at finite temperatures, the system is finite and does not have phase transitions. Instead, the system undergoes crossovers, which become phase transitions only in the thermal dynamical limit. We have verified that, numerically, as one increases M, N, the numerical data indeed tend to approach the large-N curve.

Green's function,

$$n = \frac{1}{2} + \sum_{\omega_n} G_f(i\omega_n). \tag{4}$$

Alternatively, one can obtain the filling from $n = \lim_{\delta\to 0} G(\tau = -\delta)$. However, due to the finite number of frequency points we keep, $G(\tau)$ obtained from a Fourier transform exhibits strong oscillations at small τ (the Gibbs phenomenon).

From the fermion Green's functions, we extract the n-μ curve, shown in Fig. 2. In particular, for certain values of (μ, T) the two solutions coexist, indicating the existence of metastable states. At low temperatures, there is, in general, a range of n for which no solutions were found. Nevertheless, we expect the $n(\mu)$ curve to be smooth in the full solution. This missing portion of solutions (see the dashed lines in Fig. 2) thus corresponds to those that cannot be obtained from a stable convergent iterative series. We thus identify this missing portion as thermodynamically unstable saddle points of the free energy. Such a behavior is typical of first-order phase transitions. Like water-vapor transition, the actual n-μ curve connecting the two branches is a straight line determined by the Maxwell construction. Above a certain temperature T_c, the two types of solutions become smoothly connected at a chemical potential μ_c. Here the compressibility $dn/d\mu$ diverges, and thus, (T_c, μ_c) is a thermal critical point of the system.

Qualitatively, the value of T_c up to which the first-order phase transition survives is related to the strength of the *quantum* first-order transition at $T = 0$. In Ref. [23], it was found analytically that the first-order quantum phase transition is weaker for a larger ratio M/N and becomes continuous at $M/N \to \infty$. Indeed, we find that T_c for the case $N = M$ is higher than that with $N = 4M$.

Here we note that the normal state phases of the spinless Yukawa-SYK model [24] can be obtained by a similar analysis. Indeed, the only difference is an additional factor of 2 in the second equation in (2) coming from summing over spin species. However, as we see below, the pairing phase of the spin-$\frac{1}{2}$ Yukawa-SYK model comes from the spin-singlet channel, which is absent in the spinless version, as discussed in Ref. [24].

IV. PAIRING TRANSITION

The interaction mediated by the boson exchange is attractive in the equal-index, spin-singlet Cooper channel [27], and the system has an instability and a low-temperature pairing phase. The Eliashberg equation is given by

$$\Phi(\omega_n) = \omega_0^3 T \sum_{\Omega_m} G_b(i\Omega_m) G_f[i(\omega_n + \Omega_m)] G_f[-i(\omega_n + \Omega_m)] \times \Phi(\omega_n + \Omega_m). \tag{5}$$

At $\mu = 0$, the pairing problem was analyzed in Ref. [27]. For $\mu \neq 0$, due to the breaking of particle-hole symmetry, the mismatch between $G(\pm i\omega_n)$ leads to a reduced pairing tendency, much like a Zeeman splitting in momentum space reduces the spin-singlet pairing susceptibility. We can glean some insight about the pairing transition by considering the weak-coupling limit $\omega_0 \ll m_0$ and determine the value of μ_{sc} beyond which pairing vanishes. At $T = 0$, the Schwinger-Dyson equations admit an insulating solution approximated [23] by $\Sigma(i\omega) = -\omega_F/2$, where $\omega_F \equiv \omega_0^3/m_0^2$ and $\Pi(i\Omega) = 0$ as long as $\mu > \omega_F/2$. These self-energies become exact in the limit. In this regime the pairing equation becomes

$$\Phi(\omega) = \omega_0^3 \int \frac{d\Omega}{2\pi} \frac{1}{(\Omega - \omega)^2 + m_0^2} \frac{1}{\Omega^2 + (\mu - \omega_F/2)^2} \Phi(\Omega). \tag{6}$$

Most of the support for the integral comes from frequencies on the order of ω_F, so at very weak coupling the frequency dependence of the boson propagator can be ignored. With the ansatz $\Phi(\omega) = \text{const}$, performing the integral reveals a pairing transition at

$$\mu_{sc} = \omega_F \left(\equiv \omega_0^3/m_0^2\right). \tag{7}$$

To verify this analytic result, we solved the pairing equation numerically at very weak coupling, $m_0 = 10\omega_0$, and we obtained $\mu_{sc} \approx 0.98\omega_F$ for the maximum chemical potential beyond which pairing vanishes; we also found that $\Phi(\omega)$ is virtually constant, justifying our ansatz. Extrapolating to our case with $\omega_0/m_0 = 0.5$, we expect $\mu_{sc} = 0.25$. This indeed matches well the numerical results from large N [Figs. 1(a) and 1(b)] and from QMC [Fig. 1(a)].

Using the numerical solutions for Eqs. (2), the Eliashberg equation can be viewed as a matrix equation

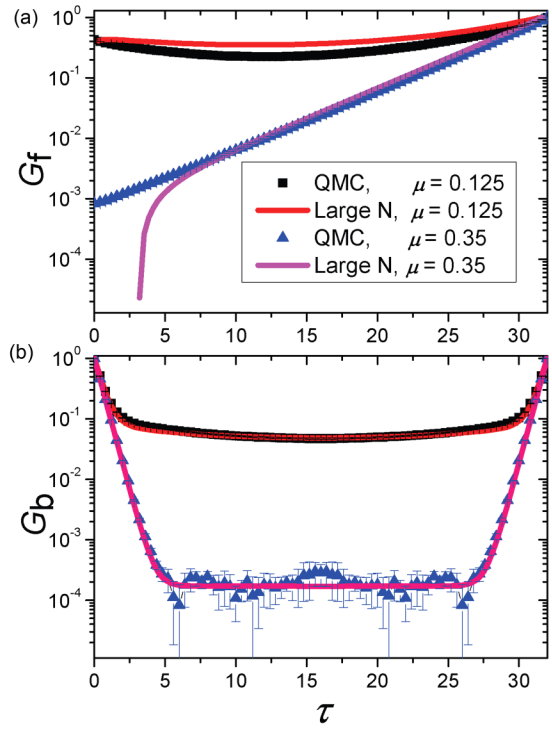

FIG. 3. (a) The QMC fermionic Green's functions and (b) the bosonic Green's functions with different μ. $M = 4$, $N = 16$, $\beta = 32$, $\omega_0 = 1$, $m_0 = 2$, plotted with semilog axes. For convenience both G_f and G_b have been normalized to 1 at $\tau = \beta$. The system becomes gapped with the increase of the chemical potential. The sharp downturn of the large-N result in (a) is an artifact of keeping finite-frequency points.

$|\Phi\rangle = \hat{K}(T,\mu)|\Phi\rangle$ (after imposing a large enough cutoff in frequency), and the largest eigenvalue of the kernel $\hat{K}$ can be computed. The Eliashberg equation has a nontrivial solution when the largest eigenvalue reaches 1, indicating the onset of pairing, and we can map out the boundary of the superconducting region in the T-μ phase diagram. The numerical results for $N = 4M, m_0 = 2\omega_0$ and $N = M, m_0 = 2\omega_0$ are shown in Figs. 1(a) and 1(b), respectively. The thermal critical point may lie inside or outside the superconducting region depending on the ratio of M/N, as discussed above.

V. RESULTS FROM QMC

To analyze the phase diagram in Fig. 1 with QMC, we focus on the Green's functions and pairing susceptibility obtained in simulations at finite M, N. We first perform the QMC simulations at the parameters of $N = 4M, \omega_0 = 1, m_0 = 2$ with different $\beta \equiv 1/T$ and μ.

We show in Fig. 3 the QMC Green's functions for large β with different μ, with $G_f(\tau,0) = \frac{1}{(MN)^2}\sum_{i,j=1}^{M}\sum_{\alpha,\beta=1}^{N}\langle c_{i,\alpha,\sigma}(\tau)c^{\dagger}_{j,\beta,\sigma}(0)\rangle$ and $G_b(\tau,0) = \frac{1}{N(N-1)}\sum_{\alpha,\beta=1,\alpha\neq\beta}^{N}\langle\phi_{\alpha\beta}(\tau)\phi_{\alpha\beta}(0)\rangle$. One can clearly see that they exhibit distinct behaviors for small and large μ, consistent with the phase diagram in Fig. 1(a). At $\mu = 0.125$, both G_f and G_b decay slowly in imaginary time, similar to the results in Ref. [27] exhibiting power-law scaling. Note that, for $\mu \neq 0$, since the system is no longer particle-hole symmetric, G_f is not symmetric with respect to $\tau = \beta/2$, and we normalize the data with respect to $G_f(\tau = \beta)$ and $G_b(\tau = \beta)$. At larger doping, with $\mu = 0.35$, both G_f and G_b decay exponentially, consistent with insulating behavior. Since in the QMC simulation with finite N, M the system does not develop superconductivity, it is sensible to compare it with Green's functions at large N for the normal state. As can be seen in Fig. 3, the agreement is excellent.

For the $M = N$ case in Fig. 1(b), the thermal critical point is located around $(\mu_c = 0.3825, T_c = 0.07)$, which is within reach of our QMC simulations. We compute the $n(\mu)$ curves (whose derivative is the charge compressibility) near and far away from T_c. We can see in Fig. 2 that, in excellent agreement with the large-N solution, the compressibility is constant when the temperature is much higher than the critical point ($M = N = 8, T = 0.125$), while there is a jump in $n(\mu)$ when the temperature is close to the critical point ($M = N = 8, 10, 12, T = 0.083$), consistent with the phase diagram in Fig. 1(b) from large N.

For $N = 4M$ our QMC results further reveal that the NFL develops a superconductivity at low temperature in a wide range of the chemical potential, reaching beyond the would-be first-order phase transition. To extract the superconducting transition temperature, we measure the pairing correlation in our QMC simulation and analyze its scaling behavior as the system size. The pair susceptibility is expressed as $P_s = \int_0^{\beta} d\tau\langle\Delta(\tau)\Delta^{\dagger}(0)\rangle$, where Δ is the pairing field defined as $\Delta^{\dagger} = \frac{1}{\sqrt{MN}}\sum_{i=1}^{M}\sum_{\alpha=1}^{N} c^{\dagger}_{i,\alpha,\uparrow}c^{\dagger}_{i,\alpha,\downarrow}$. At finite N, the pairing susceptibility P_s does not diverge and can be written as $P_s^{(N)} \sim N^a f[N^{1/\nu}(T - T_{sc})]$, in which N (and M for a fixed ratio) plays the role of the system size [8,37–39]. For our large-N system without the notion of space, the role of correlation length is replaced by a correlation "cluster size" $n \sim (T - T_{sc})^{-\nu}$ and hence the functional dependence of $f(x)$. In the large-N limit, all fluctuation effects are suppressed by $1/N$, and such a phase transition is mean-field-like [24]. This means that for a fixed $T - T_c$ the exponent $\nu = 2$ following the analog of Josephson's identity [40] and that $f(x) \sim 1/x$. Further requiring that in the large-N (thermodynamic) limit the susceptibility diverges independent of N, we obtain $a = 1/2$. Using these exponents, we indeed obtain decent finite-size scaling with β_{sc} by data collapse [see Figs. 4(a)–4(h), with different fermion densities (different μ)]. We can see that when μ increases, the superconducting transition temperature is moderately reduced until a sudden drop at larger μ. For $\mu > 0.25$ the pairing susceptibility no longer diverges with large N, and the system does not form a pairing state [see Figs. 4(i) and 4(j)]. The corresponding QMC T_{sc} points are shown in Fig. 1(a). The values of $T_{sc}(\mu)$ from QMC are

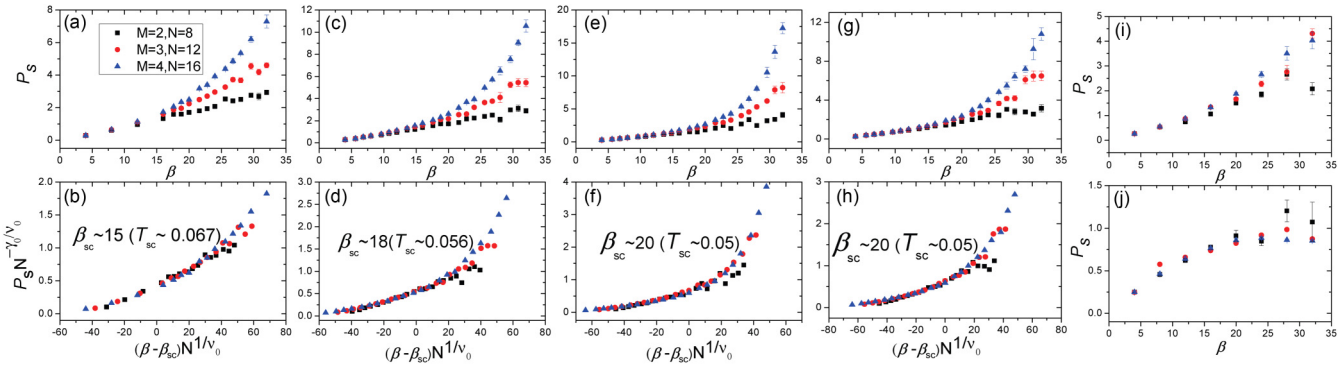

FIG. 4. Pair susceptibility P_s measured at different chemical potentials μ. The obtained T_c (β_c) are denoted by the blue triangles in Fig. 1(a). From the temperature dependence of P_s with different system sizes (M, N) we perform the data collapse using mean-field exponents $\gamma_0 = 1$, $\nu_0 = 2$, and the transition temperatures T_c (β_c) are obtained accordingly. The parameters are $N = 4M$, $\omega_0 = 1$, $m_0 = 2$. $\mu = 0$ in (a) and (b), $\mu = 0.05$ in (c) and (d), $\mu = 0.125$ in (e) and (f), $\mu = 0.2$ in (g) and (h), $\mu = 0.25$ in (i), and $\mu = 0.35$ in (j). The superconducting transition temperature decreases as μ increases. For $\mu = 0.25$ in (i) and $\mu = 0.35$ in (j) the pairing susceptibilities are not divergent at larger N, and the system enters a gapped insulator phase.

larger than their large-N counterparts, but they are close. In particular, the values of μ_{sc} from QMC and large N are in good agreement, consistent with analytical result Eq. (7).

VI. DISCUSSION

With combined analytical and numerical efforts, we revealed the T-μ phase diagram of the spin-$\frac{1}{2}$ Yukawa-SYK model. We identified that an underlying first-order quantum phase transition between a non-Fermi liquid and an insulator leads to a domelike structure of the pairing phase and, depending on the parameter N/M, survives at finite T until a second-order thermal tricritical point between a non-Fermi liquid and an insulator. The first-order quantum phase transition and the associated thermal critical point are shared by the original complex SYK model at finite density [30,31]. In addition, the superconducting dome in the vicinity of a NFL phase we observed for the spin-$\frac{1}{2}$ Yukawa-SYK model analytically and numerically in this work is reminiscent of the phase diagrams of many unconventional superconductors. Our results provide the model realization of the SYK-type NFL and its transition towards superconductivity and insulating states and therefore offer a controlled platform for future investigations of the generic phase diagram that hosts the NFL, insulator, and superconductor phases and their transitions at generic fermion densities.

It will be interesting to further investigate the scaling behavior of the thermal tricritical point and determine its universality class, which we leave for future work.

ACKNOWLEDGMENTS

We thank A. Chubukov, I. Esterlis, Y. Gu, G. Tarnopolsky, J. Schmalian, S. Sachdev, and S. Kivelson for insightful discussions. A.D. and Y.W. are supported by startup funds at the University of Florida. W.W., G.P., and Z.Y.M. acknowledge support from the RGC of Hong Kong SAR of China (Grants No. 17303019 and No. 17301420), MOST through the National Key Research and Development Program (Grant No. 2016YFA0300502), and the Strategic Priority Research Program of the Chinese Academy of Sciences (Grant No. XDB33000000). We thank the Computational Initiative at the Faculty of Science and the Information Technology Services at the University of Hong Kong and Tianhe-2 platform at the National Supercomputer Centers in Guangzhou for their technical support and generous allocation of CPU time.

APPENDIX A: MODEL AND QUANTUM MONTE CARLO SIMULATION

The Hamiltonian in Eq. (1) in the main text is illustrated by Fig. 5. There are $i, j = 1, \ldots, M$ quantum dots, and each dot acquires $\alpha, \beta = 1, \ldots, N$ flavors of fermions. Fermions are Yukawa coupled via the random hopping t_{ij} and antisymmetric bosonic field $\phi_{\alpha\beta}$. The system goes through a phase transition from a non-Fermi liquid to a pairing state when the temperature is below the superconducting critical temperature T_{sc}.

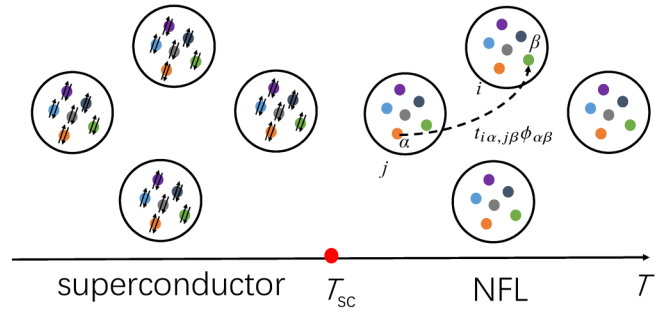

FIG. 5. Spin-$\frac{1}{2}$ Yukawa-SYK model. There are $i, j = 1, \ldots, M$ quantum dots; each dot acquires $\alpha, \beta = 1, \ldots, N$ flavors. Fermions are Yukawa coupled via the random hopping t_{ij} and antisymmetric bosonic field $\phi_{\alpha\beta}$. The system goes through a phase transition from non-Fermi liquid to a pairing state when the temperature is below the superconducting critical temperature T_{sc}.

We use the Determinantal Quantum Monte Carlo (DQMC) method to simulate this Hamiltonian, and the starting point is the partition function of the system,

$$\begin{aligned} Z &= \mathrm{Tr}\{e^{-\beta\hat{H}}\} \\ &= \mathrm{Tr}\{(e^{-\Delta\tau\hat{H}})^{L_\tau}\} \\ &= \sum_{\{\Phi\}} \mathrm{Tr}_{\mathbf{F}}\langle\Phi^1|e^{-\Delta\tau H}|\Phi^{L_\tau}\rangle\langle\Phi^{L_\tau}|e^{-\Delta\tau H}|\Phi^{L_\tau-1}\rangle \\ &\quad \times \cdots \times \langle\Phi^2|e^{-\Delta\tau H}|\Phi^1\rangle, \end{aligned} \tag{A1}$$

where we divide the imaginary-time axis β into L_τ slices; then we have $\beta = L_\tau \times \Delta\tau$. Here $\Phi_l = (\phi_{11,l}, \phi_{12,l}, \ldots, \phi_{N(N-1),l}, \phi_{NN,l})$ is the complete basis of imaginary-time propagation in the path integral. Using Trotter-Suzuki decomposition to the Hamiltonian in Eq. (A1),

$$e^{-\Delta\tau\hat{H}} \approx e^{-\Delta\tau\hat{H}_{fb}}e^{-\Delta\tau\hat{H}_b}, \tag{A2}$$

where H_{fb} is the boson-fermion term and H_b is the boson term in the Hamiltonian.

Then the partition function can be written as

$$Z = \sum_{\{\Phi\}} \omega_B[\phi]\omega_F[\phi]. \tag{A3}$$

As for the bosonic part of the partition function,

$$\begin{aligned} \omega_b[\phi] = C^{L_\tau}&\left(\prod_{l=1}^{L_\tau}\prod_{\alpha,\beta=1}^{N} e^{-\Delta\tau\frac{m_0^2}{2}\phi_{\alpha\beta,l}^2}\right) \\ &\times\left(\prod_{\langle l,l'\rangle}\prod_{\alpha,\beta=1}^{N} e^{-\frac{(\phi_{\alpha\beta,l}-\phi_{\alpha\beta,l'})^2}{2\Delta\tau}}\right), \end{aligned} \tag{A4}$$

where $\langle l, l'\rangle$ stands for the nearest-neighbor interaction in the imaginary-time direction and C is a constant. As for the fermionic part of the partition function,

$$\omega_F[\phi] = \det[I + \mathbf{B}^{L_\tau}\mathbf{B}^{L_\tau-1}\cdots\mathbf{B}^{l}\cdots\mathbf{B}^{2}\mathbf{B}^{1}], \tag{A5}$$

where

$$B^l = e^{-\Delta\tau V(\Phi_l)} \tag{A6}$$

and

$$V(\Phi_l) = \frac{i}{\sqrt{MN}}\sigma^z_{2\times 2} \otimes (t_{ij})_{M\times M} \otimes (\phi_{\alpha\beta,l})_{N\times N} - \mu \otimes \mathbb{I}_{2MN\times 2MN}. \quad \text{(A7)}$$

Here $\mathbb{I}$ is the identity matrix.

With these notations prepared, finally, the partition function in Eq. (A3) can be written as

$$Z = \sum_{\{\Phi\}}\prod_{l=1}^{L_\tau} C^{L_\tau}\left(\prod_{l=1}^{L_\tau}\prod_{\alpha,\beta=1}^{N} e^{-\Delta\tau\frac{M}{N}\frac{m_0^2}{2}\phi^2_{\alpha\beta,l}}\right) \times \left(\prod_{\langle l,l'\rangle}\prod_{\alpha,\beta=1}^{N} e^{-\frac{\left(\phi_{\alpha\beta,l}-\phi_{\alpha\beta,l'}\right)^2}{2\Delta\tau}}\right) \times \mathrm{Det}[\mathbf{I}+\mathbf{B}^{L_\tau}\mathbf{B}^{L_\tau-1}\cdots\mathbf{B}^{l}\cdots\mathbf{B}^{2}\mathbf{B}^{1}]. \quad \text{(A8)}$$

This partition function is free from the minus-sign problem for any μ. For the part of the boson-fermion term of the Hamiltonian, it is invariant under the time-reversal symmetry operation $\mathcal{T} = i\sigma_y\mathcal{K}$. Here $\mathcal{K}$ is the complex-conjugate operator. The boson-fermion term of the Hamiltonian can be written as

$$\hat{H}_{fb} = \sum_{ij=1}^{N}\sum_{\alpha,\beta=1}^{N}\frac{i}{\sqrt{MN}}t_{\alpha\beta}\phi_{ij}c^\dagger_{i\alpha\uparrow}c_{j\alpha\uparrow} - \mu c^\dagger_{i\alpha\uparrow}c_{i\alpha\uparrow} - \frac{i}{\sqrt{MN}}t_{\alpha\beta}\phi_{ij}c^\dagger_{i\alpha\downarrow}c_{j\alpha\downarrow} - \mu c^\dagger_{i\alpha\downarrow}c_{i\alpha\downarrow}. \quad \text{(A9)}$$

Under the transformation of $\mathcal{T} = i\sigma_y\mathcal{K}$, we have

$$\mathcal{T}H_{fb}\mathcal{T}^{-1} = \sum_{ij=1}^{N}\sum_{\alpha,\beta=1}^{N} -\frac{i}{\sqrt{MN}}t_{\alpha\beta}\phi_{ij}c^\dagger_{i\alpha\downarrow}c_{j\alpha\downarrow} - \mu c^\dagger_{i\alpha\downarrow}c_{i\alpha\downarrow} + \frac{i}{\sqrt{MN}}t_{\alpha\beta}\phi_{ij}c^\dagger_{i\alpha\uparrow}c_{j\alpha\uparrow} - \mu c^\dagger_{i\alpha\uparrow}c_{i\alpha\uparrow} = H_{fb}. \quad \text{(A10)}$$

At the same time for the fermion determinant

$$\begin{aligned}&\det[1+B(\beta,0)]\\ &= \det[1+B^\uparrow(\beta,0)]\det[1+B^\downarrow(\beta,0)]\\ &= \det[1+B^\uparrow(\beta,0)]\det[\mathcal{T}(1+B^\downarrow(\beta,0))\mathcal{T}^{-1}]^*\\ &= \det[1+B^\uparrow(\beta,0)]\det[1+B^\uparrow(\beta,0)]^* \quad \text{(A11)}\\ &= |\det[1+B^\uparrow(\beta,0)]|^2, \quad \text{(A12)}\end{aligned}$$

where $B(\beta,0) = \mathbf{B}^{L_\tau}\mathbf{B}^{L_\tau-1}\cdots\mathbf{B}^{l}\cdots\mathbf{B}^{2}\mathbf{B}^{1}$. The determinant is a positive and real number. Also for the boson part of the weight $\omega_b[\phi]$ is positive and real. Therefore, we have proved that this Hamiltonian is sign problem free.

From a simpler viewpoint, just by looking at the matrix elements of matrices corresponding to different spins, $B^\uparrow(\beta,0)$ and $B^\downarrow(\beta,0)$, we can see this model does not have sign problem. Every element of $1+B^\downarrow(\beta,0)$ is individually complex conjugate with the corresponding element of $1+B^\uparrow(\beta,0)$, which means

$$\det[1+B^\uparrow(\beta,0)] = \det[1+B^\downarrow(\beta,0)]^*. \quad \text{(A13)}$$

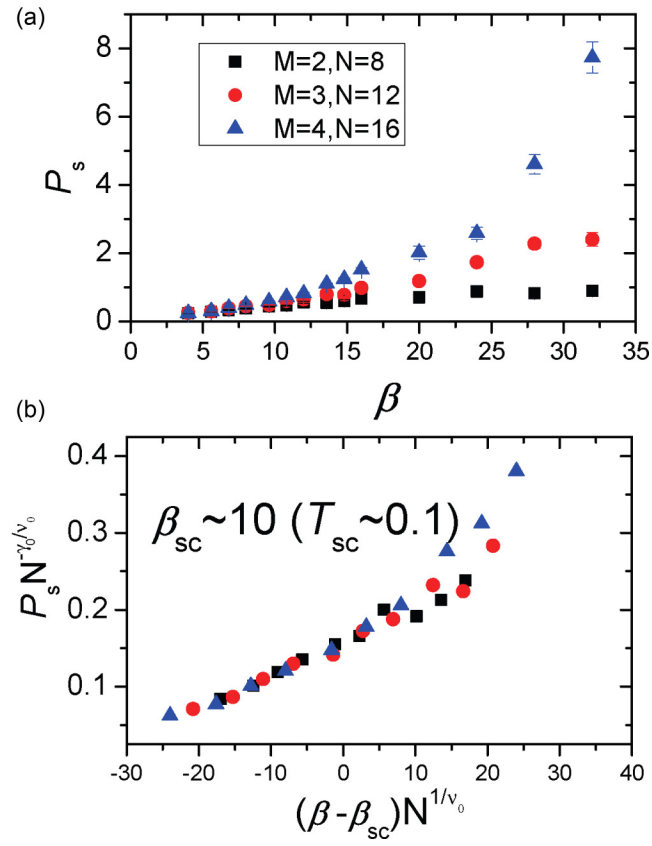

FIG. 6. Pair susceptibility for different β and data collapse, $\omega_0 = 1$, $m_0 = 1$, $\mu = 0$. The superconducting transition temperature is around $T_{sc} \sim 0.1$ ($\beta_c \sim 10$), which is higher than the superconducting transition temperature around $T_{sc} \sim 0.067$ ($\beta_{sc} \sim 15$) at $\omega_0 = 1$, $m_0 = 2$, and $\mu = 0$.

APPENDIX B: THE CRITICAL TEMPERATURE OF SUPERCONDUCTING WITH DIFFERENT m_0

The influence of the ratio ω_0/m_0 on the superconducting transition temperature has been studied quantitatively by the large-N limit calculation. The inverse transition temperature β_c from NFL to superconductivity as a function of the ratio ω_0/m_0 for $N = 4M$ and $N = M$ is discussed in the main text and in Ref. [27]. By QMC simulation, we also found that when $m_0 = 1$, $\omega_0 = 1$, and $\mu = 0$, the superconducting transition temperature is around $T_{sc} \sim 0.1$ ($\beta_{sc} \sim 10$), which is higher than the superconducting transition temperature around $T_{sc} \sim 0.067$ ($\beta_{sc} \sim 15$) at $\omega_0 = 1, m_0 = 2$, and $\mu = 0$. The results are shown in Fig. 6 and are consistent with theoretical analysis in Ref. [27].

[1] B. Keimer, S. A. Kivelson, M. R. Norman, S. Uchida, and J. Zaanen, From quantum matter to high-temperature superconductivity in copper oxides, Nature (London) **518**, 179 (2015).

[2] Z. Liu, Y. Gu, W. Zhang, D. Gong, W. Zhang, T. Xie, X. Lu, X. Ma, X. Zhang, R. Zhang, Jun Zhu, C. Ren, L. Shan, X. Qiu, P. Dai, Y. Yang, H. Luo, and S. Li, Nematic Quantum Critical

Fluctuations in $BaFe_{2-x}Ni_xAs_2$, Phys. Rev. Lett. **117**, 157002 (2016).

[3] Y. Gu, Z. Liu, T. Xie, W. Zhang, D. Gong, D. Hu, X. Ma, C. Li, L. Zhao, L. Lin, Z. Xu, G. Tan, G. Chen, Z. Yang Meng, Y. Yang, H. Luo, and S. Li, Unified Phase Diagram for Iron-Based Superconductors, Phys. Rev. Lett. **119**, 157001 (2017).

[4] J. Custers, P. Gegenwart, H. Wilhelm, K. Neumaier, Y. Tokiwa, O. Trovarelli, C. Geibel, F. Steglich, C. Pépin, and P. Coleman, The break-up of heavy electrons at a quantum critical point, Nature (London) **424**, 524 (2003).

[5] B. Shen, Y. Zhang, Y. Komijani, M. Nicklas, R. Borth, A. Wang, Y. Chen, Z. Nie, R. Li, X. Lu, H. Lee, M. Smidman, F. Steglich, P. Coleman, and H. Yuan, Strange-metal behaviour in a pure ferromagnetic Kondo lattice, Nature (London) **579**, 51 (2020).

[6] Y. Cao, D. Chowdhury, D. Rodan-Legrain, O. Rubies-Bigorda, K. Watanabe, T. Taniguchi, T. Senthil, and P. Jarillo-Herrero, Strange Metal in Magic-Angle Graphene with Near Planckian Dissipation, Phys. Rev. Lett. **124**, 076801 (2020).

[7] C. Shen, Y. Chu, Q. S. Wu, N. Li, S. Wang, Y. Zhao, J. Tang, J. Liu, J. Tian, K. Watanabe, T. Taniguchi, R. Yang, Z. Y.g Meng, D. Shi, Oleg V. Yazyev, and G. Zhang, Correlated states in twisted double bilayer graphene, Nat. Phys. (2020).

[8] C. Chen, T. Yuan, Y. Qi, and Z. Y. Meng, Doped orthogonal metals become Fermi arcs, Phys. Rev. B **103**, 165131 (2021).

[9] S. Sachdev and J. Ye, Gapless Spin-Fluid Ground State in a Random Quantum Heisenberg Magnet, Phys. Rev. Lett. **70**, 3339 (1993).

[10] A Kitaev (unpublished).

[11] S. Sachdev, Bekenstein-Hawking Entropy and Strange Metals, Phys. Rev. X **5**, 041025 (2015).

[12] A. Kitaev and S. J. Suh, The soft mode in the Sachdev-Ye-Kitaev model and its gravity dual, J. High Energy Phys. 05 (2018) 183.

[13] A. Abanov, A. Chubukov, and J. Schmalian, Quantum-critical theory of the spin-fermion model and its application to cuprates: Normal state analysis, Adv. Phys. **52**, 119–218 (2003).

[14] M. A. Metlitski and S. Sachdev, Quantum phase transitions of metals in two spatial dimensions. I. Ising-nematic order, Phys. Rev. B **82**, 075127 (2010).

[15] M. A. Metlitski and S. Sachdev, Quantum phase transitions of metals in two spatial dimensions. II. Spin density wave order, Phys. Rev. B **82**, 075128 (2010).

[16] Z. H. Liu, X. Y. Xu, Y. Qi, K. Sun, and Z. Y. Meng, Itinerant quantum critical point with frustration and a non-Fermi liquid, Phys. Rev. B **98**, 045116 (2018).

[17] Z. H. Liu, G. Pan, X. Y. Xu, K. Sun, and Z. Y. Meng, Itinerant quantum critical point with fermion pockets and hotspots, Proc. Natl. Acad. Sci. U.S.A. **116**, 16760 (2019).

[18] X. Y. Xu, Z. H. Liu, G. Pan, Y. Qi, K. Sun, and Z. Y. Meng, Revealing fermionic quantum criticality from new Monte Carlo techniques, J. Phys.: Condens. Matter **31**, 463001 (2019).

[19] X. Y. Xu, A. Klein, K. Sun, A. V. Chubukov, and Z. Y. Meng, Identification of non-Fermi liquid fermionic self-energy from quantum Monte Carlo data, npj Quantum Mater. **5**, 65 (2020).

[20] J. Aguilera Damia, M. Solís, and G. Torroba, How non-Fermi liquids cure their infrared divergences, Phys. Rev. B **102**, 045147 (2020).

[21] H. Guo, Y. Gu, and S. Sachdev, Linear in temperature resistivity in the limit of zero temperature from the time reparameterization soft mode, Ann. Phys. (NY), **418** 168202 (2020).

[22] Y. Gu, X.-L. Qi, and D. Stanford, Local criticality, diffusion and chaos in generalized Sachdev-Ye-Kitaev models, J. High Energy Phys. 05 (2017) 125.

[23] Y. Wang and A. V. Chubukov, Quantum phase transition in the Yukawa-SYK model, Phys. Rev. Res. **2**, 033084 (2020).

[24] Y. Wang, Solvable Strong-Coupling Quantum-Dot Model with a Non-Fermi-Liquid Pairing Transition, Phys. Rev. Lett. **124**, 017002 (2020).

[25] I. Esterlis and J. Schmalian, Cooper pairing of incoherent electrons: An electron-phonon version of the Sachdev-Ye-Kitaev model, Phys. Rev. B **100**, 115132 (2019).

[26] D. Hauck, M. J. Klug, I. Esterlis, and J. Schmalian, Eliashberg equations for an electron–phonon version of the Sachdev–Ye–Kitaev model: Pair breaking in non-Fermi liquid superconductors, Ann. Phys. (NY) **417**, 168120 (2020).

[27] G. Pan, W. Wang, A. Davis, Y. Wang, and Z. Y. Meng, Yukawa-SYK model and self-tuned quantum criticality, Phys. Rev. Res. **3**, 013250 (2021).

[28] J. Kim, X. Cao, and E. Altman, Low-rank Sachdev-Ye-Kitaev models, Phys. Rev. B **101**, 125112 (2020).

[29] J. Kim, E. Altman, and X. Cao, Dirac fast scramblers, Phys. Rev. B **103**, L081113 (2021).

[30] T. Azeyanagi, F. Ferrari, and F. I. Schaposnik Massolo, Phase Diagram of Planar Matrix Quantum Mechanics, Tensor, and Sachdev-Ye-Kitaev Models, Phys. Rev. Lett. **120**, 061602 (2018).

[31] R. Smit, D. Valentinis, J. Schmalian, and P. Kopietz, Quantum discontinuity fixed point and renormalization group flow of the SYK model, arXiv:2010.01142.

[32] H. Wang, A. L. Chudnovskiy, A.r Gorsky, and A. Kamenev, Sachdev-Ye-Kitaev superconductivity: Quantum Kuramoto and generalized Richardson models, Phys. Rev. Res. **2**, 033025 (2020).

[33] C. Setty, Pairing instability on a Luttinger surface: A non-Fermi liquid to superconductor transition and its Sachdev-Ye-Kitaev dual, Phys. Rev. B **101**, 184506 (2020).

[34] Y. Cheipesh, A. I. Pavlov, V. Scopelliti, J. Tworzydło, and N. V. Gnezdilov, Reentrant superconductivity in a quantum dot coupled to a Sachdev-Ye-Kitaev metal, Phys. Rev. B **100**, 220506(R) (2019).

[35] M. Imada, A. Fujimori, and Y. Tokura, Metal-insulator transitions, Rev. Mod. Phys. **70**, 1039 (1998).

[36] P. Limelette, A. Georges, D. Jérome, P. Wzietek, P. Metcalf, and J. M. Honig, Universality and critical behavior at the Mott transition, Science **302**, 89 (2003).

[37] S. V. Isakov and R. Moessner, Interplay of quantum and thermal fluctuations in a frustrated magnet, Phys. Rev. B **68**, 104409 (2003).

[38] T. Paiva, R. R. dos Santos, R. T. Scalettar, and P. J. H. Denteneer, Critical temperature for the two-dimensional

attractive Hubbard model, Phys. Rev. B **69**, 184501 (2004).

[39] N. C. Costa, T. Blommel, W.-T. Chiu, G. Batrouni, and R. T. Scalettar, Phonon Dispersion and the Competition Between Pairing and Charge Order, Phys. Rev. Lett. **120**, 187003 (2018).

[40] For a mean-field theory in finite spatial dimensions, Josephson's identity states that $\nu d = 2$, and in our model the dimensionality d does not enter the theory. We have instead $\nu = 2$. We thank I. Esterlis and J. Schmalian for sharing their unpublished results with us on this.